JOURNAL OF SPACECRAFT AND ROCKETS
Vol. 47, No. 2, March–April 2010

Effects of Variations in Plasma Propulsion System Performance on Mars Cargo Missions

Kamesh Sankaran,* Kellen Oetgen, Marc Rollins, and Evan Staley
Whitworth University, Spokane, Washington 99251

DOI: 10.2514/1.47074

The results of a study to analyze the effects of variations in a lithium Lorentz force accelerator propulsion system performance on a mission to Mars are presented. The total mass and the trip time required to transport a fixed payload (9000 kg) from low Earth orbit to Mars orbit for various combinations of specific mass of the power plant (from 4 to 64 kg/kW), input power (from 100 to 1000 kW), efficiency (from 30 to 75%), and either exhaust velocity (from 30 to 60 km/s) or mass flow rate (from 0.05 to 0.60 g/s) were calculated by integrating the equations of motion of the spacecraft. The variations considered in this study were close to experimentally demonstrated values of performance parameters of a plasma thruster. The results indicate a point of diminishing return above which large increases in input power are necessary for modest decreases in trip time. The results show the existence of an optimum input power at which the total mass required is at a minimum. They also reveal the optimum exhaust velocity that minimizes the total spacecraft mass, for a given propellant flow rate and specific mass. At a given power level, there exists an optimum exhaust velocity that minimizes trip time as well. The total trip time decreases strongly with increasing efficiency, indicating the importance of research into increasing thruster efficiency.

Nomenclature

a	=	acceleration, m/s^2
G	=	gravitational constant, N.m^2/kg^2
h	=	specific angular momentum, m/s
M_e	=	mass of the Earth, kg
M_{fix}	=	fixed mass, kg
M_{pay}	=	payload mass, kg
M_{pp}	=	powerplant mass, kg
M_{prop}	=	propellant mass, kg
M_{tot}	=	total mass, kg
$\dot{m}$	=	propellant flow rate, g/s
P_{in}	=	input power, kW
P_{th}	=	thruster power, kW
r	=	radial distance, m
T	=	thrust, N
t_{escape}	=	time in Earth escape phase, s
t_{helio}	=	time in heliocentric phase, s
t_{capture}	=	time in Mars capture phase, s
u_{ex}	=	exhaust velocity, km/s
$\hat{u}_{\text{ex}}$	=	optimum exhaust velocity, km/s
v_r	=	radial velocity of the spacecraft, m/s
v_θ	=	azimuthal velocity of the spacecraft, m/s
α	=	specific mass, kg/kW
η	=	thruster efficiency, %
μ	=	$G\times$ mass of the central gravitational body
ϕ	=	thrust angle, rad

I. Motivation and Background

ELECTRIC propulsion (EP) systems become attractive for cargo and piloted missions to Mars with the availability of onboard electric power of $\mathcal{O}(100)$ kW or more. Numerous studies have analyzed missions to Mars since the early days of EP [1–3]. Recently, Chiravalle [4] analyzed this mission using nuclear electric ion propulsion and demonstrated significant mass savings. Sankaran et al. [5] analyzed several propulsion systems based on their measured performance data, and found that the lithium Lorentz force accelerator (LiLFA) was an excellent candidate for such missions.

However, there exists a need to quantify the effects of variations in the performance parameters of such a thruster and other necessary components of the propulsion system, such as the onboard power supply, on the overall mission. This has implications both for planning the mission and for providing directions for research and development. The objective of this study is to partially meet that need by exploring these variations within a range of performance parameters that are reasonably close to experimentally demonstrated values. It is not the goal of this study to accurately predict the values of total spacecraft masses, trip times, or optimum exhaust velocities, but the goal is to study how those quantities vary with variations in the performance of the propulsion system.

II. Assumptions

In this study, calculation of the trajectory of a one-way trip from Earth to Mars was done in three sequential phases: the Earth escape, the heliocentric cruise, and the Mars capture. In each phase the spacecraft was considered to be in the sphere of influence of only one central gravitational field. In the Earth escape phase, the spacecraft spirals around the earth until it reaches the local escape velocity. In the heliocentric cruise, the spacecraft travels outward around the sun and in the Mars capture phase, the spacecraft spirals inward to the desired altitude above Mars.

The spacecraft's mission was assumed to begin at 500 km low Earth orbit (LEO) and end at an orbit 1500 km above Mars. Both Mars and Earth were considered to have coplanar concentric circular orbits about the sun, as in [4,6,7]. Because of the earlier results of Sankaran et al. [5], this study will start with the measured performance data of LiLFA used in [5] as the baseline, and the effects of variation from this baseline on the mission are analyzed.

The specific mass was allowed to vary from 4 to 64 kg/kW to reflect the variety of existing and proposed space power supply systems [8,9]. The exhaust velocity was allowed to vary from 30 to 60 km/s. The propellant mass flow rate was allowed to vary from 0.05 to 0.60 g/s. It is important to note that the efficiency is not independent of the input power. In this study, we use a predicted variation of efficiency with power for various values of u_{ex} and $\dot{m}$, from [10], shown in Fig. 1 (note that [10] uses the symbol m to denote propellant flow rate). This figure shows how the efficiency of the LiLFA would vary with input power, depending on the propellant flow rate and the exhaust velocity. It shows that at a given exhaust

Received 7 September 2009; revision received 22 January 2010; accepted for publication 25 January 2010.

*Associate Professor, Physics Department. Senior Member AIAA.

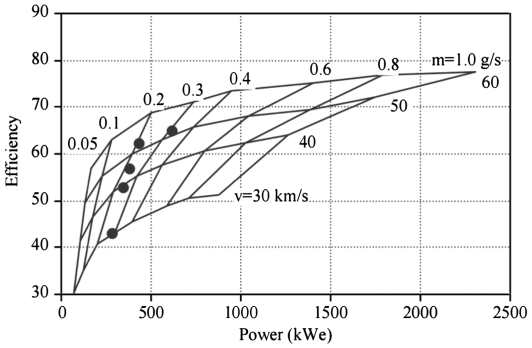

Fig. 1 Predicted LiLFA performance parameters, with some measured values [10].

velocity, the efficiency would increase with input power, and at a given power level, the efficiency would increase with exhaust velocity. In Sec. III we discuss how the other propulsive parameters are obtained from Fig. 1 and the relationship between input power, thrust power, exhaust velocity, and propellant flow rate [Eqs. (2) and (3)].

The input power ranged from 100 to 1000 kW and, in accordance with the trends shown in Fig. 1, the resulting efficiencies ranged from about 30 to 75%. The thrust, propellant flow rate, exhaust velocity, input power, and thruster efficiency were all calculated self-consistently from the other determined values and held constant throughout the duration of the mission. The payload to be carried was fixed at 9000 kg. This was done to allow comparison with [5]. Though the results in [5] were obtained using the RAPTOR code developed by the NASA Johnson Space Center that did not assume concentric circular orbits, repeating those calculations with this assumption only led to errors that were less than 2%. It is worth noting again that it is not the goal of this study to provide accurate predictions for values of total spacecraft mass or trip time, nor is it to provide true optimum values for exhaust velocity, but only to look at how those quantities vary with variations in the performance of the propulsion system.

III. Estimation of Relevant Parameters

From the four primary thruster parameters (α, η, and P_{in}), the other necessary parameters can be calculated. The mass of the powerplant is calculated using the specific mass of the power supply and the total input power

$$M_{\text{pp}} = \alpha P_{\text{in}} \tag{1}$$

The thrust power output by the thrusters is calculated as

$$P_{\text{th}} = \eta P_{\text{in}} \tag{2}$$

For a given exhaust velocity, the propellant flow rate is calculated to be

$$\dot{m} = 2\frac{P_{\text{th}}}{u_{\text{ex}}^2} \tag{3}$$

For a given massflow rate, the propellant flow rate is calculated to be

$$u_{\text{ex}} = \sqrt{2\frac{P_{\text{th}}}{\dot{m}}} \tag{4}$$

Knowing both $\dot{m}$ and u_{ex}, the thrust can be calculated as

$$T = \dot{m}u_{\text{ex}} \tag{5}$$

Each simulation begins with a guess for the total trip time, as well as the times for each of the three phases. From the total trip time the fuel mass can be calculated using the following equation:

$$M_{\text{prop}} = \dot{m}t_{\text{tot}} \tag{6}$$

Based on the estimates in [5,9], the fixed mass of the spacecraft, including structure, thruster, etc., is assumed to be 4% of the sum of fuel, power plant, and payload masses

$$M_{\text{fix}} = 0.04(M_{\text{pp}} + M_{\text{prop}} + M_{\text{pay}}) \tag{7}$$

This results in the total mass to be

$$M_{\text{tot}} = M_{\text{prop}} + M_{\text{fix}} + M_{\text{pp}} + M_{\text{pay}} \tag{8}$$

The initial acceleration of the spacecraft is calculated as

$$a_{\circ} = \frac{T}{M_{\text{tot}}} \tag{9}$$

The heliocentric phase's initial acceleration is calculated the same way but the acceleration is higher due to the lower total mass. The capture phase is calculated as the reverse of escape from Mars, and therefore the initial acceleration at Mars orbit must be specified. It is assumed that the spacecraft uses up all of its fuel on the mission, so that the only mass left is the structural mass, payload, and powerplant mass. Therefore, because the thrust is constant, the initial acceleration can be written as

$$a_{\circ,\text{capture}} = \frac{T}{M_{\text{tot}} - M_{\text{prop}}} \tag{10}$$

A. Equations of Motion

The equations of motion of the spacecraft are

$$\frac{\mathrm{d}r}{\mathrm{d}t} = v_r \tag{11}$$

$$\frac{\mathrm{d}v_r}{\mathrm{d}t} = \frac{h^2}{r^3} - \frac{\mu}{r^2} + a\sin\phi \tag{12}$$

$$\frac{\mathrm{d}h}{\mathrm{d}t} = ra\cos\phi \tag{13}$$

where the first equation calculates the change in orbit radius with time, the second determines the change in radial velocity with time, and the final equation calculates the change in specific angular momentum with time. Here, μ is the product of the gravitational constant and the mass of the central gravitational body. Following the method used in [4], the acceleration of the spacecraft was found from the equation below where $s = +1$ for the capture phase and $s = -1$ for the escape and heliocentric phase

$$a(t) = \frac{a_{\circ}}{1 + s\frac{a_{\circ}t}{u_{\text{ex}}}} \tag{14}$$

B. Initial Conditions

1. Earth Escape

The spacecraft begins from a 500 km LEO where the Earth is the only gravitational body considered to be acting upon the spacecraft. The initial radial velocity is set to zero. The specific angular momentum is

$$h = rv_{\theta} \tag{15}$$

where the angular velocity is

$$v_{\theta} = \sqrt{\frac{GM_e}{r}} \tag{16}$$

2. Heliocentric Cruise

In this phase the sun is the only gravitational body that affects the motion. The initial radius value is now the distance between the Earth and the sun, plus the distance from the spacecraft to the Earth. The radial velocity of the spacecraft is the same as the final value at Earth escape, but the angular velocity is different. It is now the sum of the angular velocities of the spacecraft relative to the Earth and the angular velocity of the Earth relative to the sun. The latter is

calculated based on how long it takes the Earth to make a full revolution about the sun in seconds, assuming a circular orbit, leading to a calculated value of $v_\theta \simeq 30$ km/s.

3. Mars Capture

In this phase Mars is the gravitational body that affects the motion. Chiravalle [4] showed that the capture phase can be calculated as the reverse of escape, but the s coefficient in Eq. (14) for the acceleration is now positive because the spacecraft spirals inward. Therefore, in this study the Mars capture phase was calculated in reverse and treated as an escape phase starting at the final destination of 1500 km above Mars.

The initial radial velocity is again set to zero because the final destination is for the spacecraft to be circularly orbiting Mars. The initial acceleration is found from the empty mass, using Eq. (10), because it is assumed that all of the fuel taken is used up along the mission and the thrust is considered constant throughout the entire mission.

C. Thrust Angle

Integration of Eqs. (11–13) requires that the thrust angle ϕ be specified. In this work, the thrust angle was allowed to vary during the mission. Chiravalle [4] performs this variation with a fixed heliocentric cruise time and then finds the thrust angle using a tenth-order polynomial fit. Because the purpose of this study is not to optimize the trip but rather to understand the effect of relevant performance parameters on the mission, this study will use a simpler estimation for $\phi(t)$: a sinusoidal variation with an amplitude of $\pm\pi/4$. The equations used are listed below for each phase, where t is reset to 0 at the start of each phase

$$\phi_{\text{escape}}(t) = \frac{\pi}{4}\sin\left(\frac{\pi}{t_{\text{escape}}}t\right) \tag{17}$$

$$\phi_{\text{helio}}(t) = \frac{\pi}{4}\sin\left(\frac{2\pi}{t_{\text{helio}}}t\right) \tag{18}$$

$$\phi_{\text{capture}}(t) = -\frac{\pi}{4}\sin\left(\frac{\pi}{t_{\text{capture}}}t\right) \tag{19}$$

A number of planetary masses and distances were needed for the calculations. They are listed in Table 1. These values were used to determine the initial conditions for each phase as well.

D. Low-Thrust Trajectory Calculation

A fourth-order Runge–Kutta method with $\Delta t \sim \mathcal{O}(0.1)$ s was used to simultaneously integrate Eqs. (11–13). This advances the spacecraft in time from Earth orbit to Mars orbit and thus calculates the trajectory of the spacecraft.

As mentioned earlier, each simulation begins with a guess for total trip time (and thus the total fuel mass and hence the total mass), as well as individual phase times. Starting with these guesses for trip and phase times, the equations of motions Eqs. (11–13) are integrated simultaneously, with the spacecraft starting from Earth orbit, until it reaches the Mars orbit. This yields the calculated values of total and phase trip times. These were compared with the initial guess values and the guess values were altered automatically with a new guess that was halfway in between the calculated value and the old guess, and a new mission simulation was started. This process is repeated until the difference between the guess times and the calculated times was less than 0.1% for each phase and for the total phase.

Table 1 Constant masses and distances

Radii	
Earth	6.378×10^6 m
Mars	3.396×10^6 m
Average distances	
Sun–Earth	1.49×10^{11} m
Sun–Mars	2.07×10^{11} m
Masses	
Earth	5.9736×10^{24} kg
Mars	6.4185×10^{23} kg
Sun	1.9891×10^{30} kg

IV. Results and Analysis

To understand the effect of variations in the performance of the LiLFA and the specific mass of the power plant, 611 distinct cases of the one-way mission from Earth orbit to Mars orbit were simulated, each with a specific set of α, P_{in}, η, and either u_{ex} or $\dot{m}$. Depending upon the initial guesses, this process required about 20 iterations for each data point. The results of those calculations are discussed in the following subsections.

A. Constant Exhaust Velocity

A set of trajectory calculations were done by setting α, P_{in}, η, and u_{ex} [with $\dot{m}$ determined from P_{th} and u_{ex} using Eq. (3)]. These are simulations along constant exhaust velocity lines in Fig. 1. Along each of the four lines ($u_{\text{ex}} = 30$, 40, 50, and 60 km/s), the thruster efficiency was related to the input power with analytical expressions for $\eta(P_{\text{in}}; u_{\text{ex}})$ that fit the corresponding curves in Fig. 1.

A plot of the total mass of the spacecraft as a function of the input power for various values of exhaust velocity at different values of specific mass of the power plant is shown in Fig. 2. Within the range of power levels examined (100–750 kW), the total mass appears to increase nearly linearly with the input power. This is because under the assumption of constant exhaust velocity, an increase in input power translates into a linear increase in the propellant flow rate [cf. Eq. (3)], as well as a linear increase in the mass of the power-plant, along with a corresponding increase in the fixed mass. It is worth noting that the data points in the $\alpha = 4$ kg/kW case, for $P_{\text{in}} < 150$ kW, do not fit as well with the trendline as the data points for higher power levels. If the trip time increases significantly at lower power levels ($P_{\text{in}} < 150$ kW), it would increase the propellant mass required and this trend seen in the higher power levels may no longer be true. Therefore, further investigations are required to predict this curve at those low power levels.

A plot of the trip time as a function of the input power for various values of exhaust velocity at different values of specific mass of the power plant is shown in Fig. 3. It shows that, despite the increase in the mass of the spacecraft (Fig. 2) the trip time decreases monotonically with increasing input power under these assumptions. It is also seen that there is an effective horizontal asymptote, an effective lower bound for the trip time at or near which the input power needs to increase significantly to have even a modest reduction in trip time.

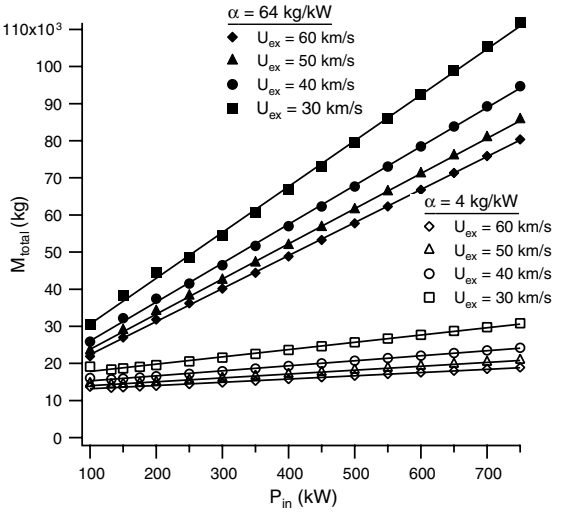

Fig. 2 Mass of the spacecraft as a function of input power for various values of exhaust velocity at two values of specific mass of the powerplant.

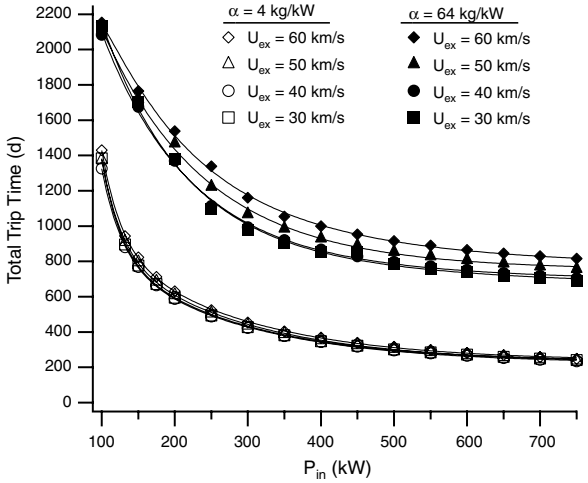

Fig. 3 Trip time as a function of input power for various values of exhaust velocity at two values of specific mass of the powerplant.

As expected, the trip times for $\alpha = 64$ kg/kW are significantly higher than those for $\alpha = 4$ kg/kW. At each power level and α, higher exhaust velocity cases had higher values for trip times than the ones with lower exhaust velocities. Moreover, the variation in trip time with exhaust velocity (at a specified value of power) was larger for larger values of α.

A plot of the trip time as a function of the efficiency of the thruster for various values of exhaust velocity at different values of specific mass of the powerplant is shown in Fig. 4. It shows that the trip time decreases sharply with increasing efficiency. This result is a combination of the increased input power needed to attain the higher values of efficiency, as well as the reduction in the powerplant mass with the higher efficiency that leads to higher acceleration of the spacecraft. It is also seen that there is an effective horizontal asymptote, but the effect is not as clear as in Fig. 3.

B. Constant Propellant Flow Rate

Next, a set of trajectory calculations were done by setting α, P_{th}, η, and $\dot{m}$ [with u_{ex} determined from P_{th} and $\dot{m}$ using Eq. (4)]. These are simulations along constant mass flow rate lines in Fig. 1. Along each of these lines ($\dot{m} = 0.05, 0.10, 0.20, 0.30, 0.40, 0.60$ g/s), the thruster efficiency was related to the input power with analytical expressions for $\eta(P_{\text{in}}; \dot{m})$ that fit the corresponding curves in Fig. 1.

Figure 5 shows the variation in total spacecraft mass with exhaust velocity for two values of propellant mass flow rate at different values of specific mass of the powerplant. It shows the existence of an optimum exhaust velocity [3] at which the total spacecraft mass M_{tot} is at a minimum. Ignoring the mass of the payload and the fixed mass in Eq. (8), Jahn [3] estimates the optimum exhaust velocity for a given trip as that which leads to the lowest sum of propellant mass and powerplant mass. This occurs when $M_{\text{prop}} = M_{\text{pp}}$, leading to

$$\hat{u}_{\text{ex}} = \sqrt{\frac{2\eta t_{\text{tot}}}{\alpha}} \tag{20}$$

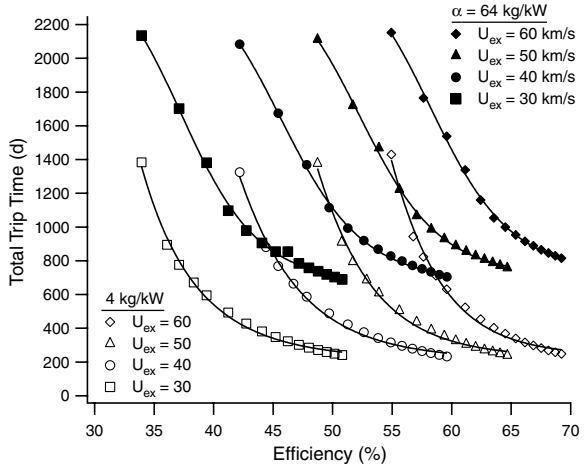

Fig. 4 Total trip time vs thruster efficiency for various exhaust velocities at two values of specific mass of the powerplant.

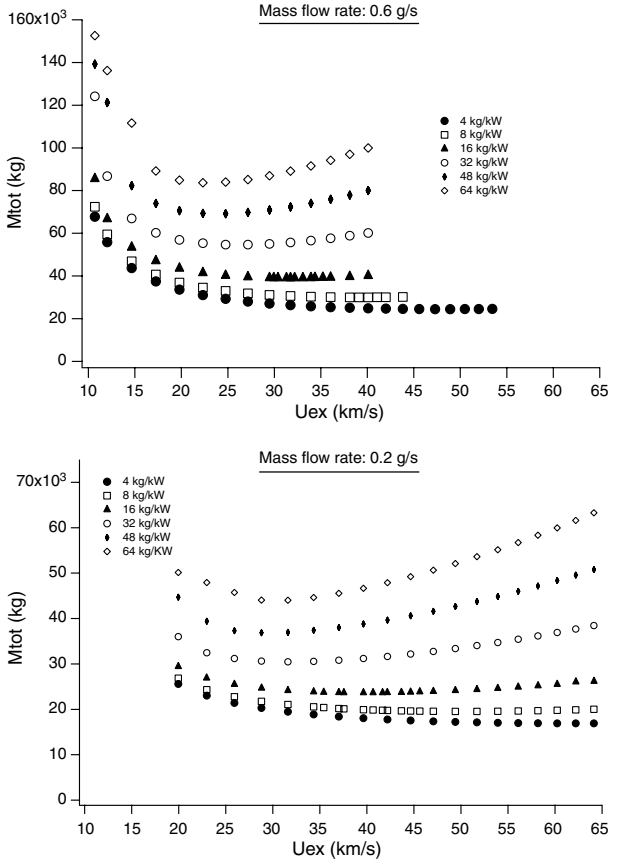

Fig. 5 Mass of the spacecraft vs the exhaust velocity for two values of propellant mass flow rate at various values of specific mass of the power plant.

As predicted [3] in Eq. (20), the optimum exhaust velocities shown in Fig. 5 decrease with increasing values of α. The approximate optimum exhaust velocities $\hat{u}_{\text{ex}}$ from the data shown in Fig. 5 for various values of specific mass of the powerplant, at three different mass flow rates, are listed in Table 2. Because of the finite resolution of the discrete variation in values used for simulating the mission, the optimum exhaust velocity can only be determined to be within a range of values, in contrast to a true optimum that can be obtained from an analytical function.

According to the theoretical prediction in Eq. (20), the optimum exhaust velocity should not vary with the propellant mass flow rate. However, Fig. 5 and the associated Table 2 show that the optimum exhaust velocity decreases with increasing mass flow rate. This is because Eq. (20) assumes the efficiency of the thruster η to be independent of the input power. However, in this study we account for the variation of efficiency with power, as predicted in [10]. As shown in Fig. 1, at a given value of input power the efficiency decreases with increasing propellant flow rate. Therefore, the propellant flow rate affects the optimum exhaust velocity.

The lowest values of total spacecraft mass, corresponding to the optimum exhaust velocities listed in Table 2, are shown in Table 3. They show that the minimum total spacecraft mass M_{tot} increases with increasing value of the specific mass of the powerplant α, and that the minimum M_{tot} also increases with increasing propellant flow rate.

Table 2 Optimum exhaust velocities at three propellant flow rates for various values of power plant specific mass

$\dot{m}$, g/s	$\hat{u}_{ex}$, km/s at various values of α					
	$\alpha = 4$ kg/kW	8 kg/kW	16 kg/kW	32 kg/kW	48 kg/kW	64 kg/kW
0.20	60.3–62.3	47.4–49.8	38.0–39.8	29.8–32.6	26.5–29.4	$\simeq$ 28.8
0.30	56.7–59.3	44.3–47.0	36.0–37.3	27.6–31.7	26.7–27.4	26.2–26.7
0.60	48.7–50.3	38.4–39.4	32.2–33.0	27.0–29.3	24.4–26.8	20.3–22.8

Table 3 Lowest spacecraft mass at three propellant flow rates for various values of power plant specific mass

$\dot{m}$, g/s	M_{tot}, $\times 10^3$ kg at various values of α					
	$\alpha = 4$ kg/kW	8 kg/kW	16 kg/kW	32 kg/kW	48 kg/kW	64 kg/kW
0.20	16.91	19.55	23.68	30.48	36.85	$\simeq$ 44.0
0.30	19.01	22.37	27.78	36.87	45.33	54.02
0.60	24.47	30.00	39.06	54.67	69.20	83.65

Figure 6 shows how the total spacecraft mass varies with input power, at two different values of propellant mass flow rate at different values of specific mass of the power plant. This shows that there exists an optimum power that results in the lowest total mass of the spacecraft. The reason for the existence of an optimum input power that minimizes total mass is this: under the condition of constant propellant flow rate, varying power means varying the exhaust velocity [cf. (3)]; therefore, just as there exists an optimum exhaust velocity that minimizes total mass, there also exists a corresponding optimum power level that minimizes total mass, as seen in Fig. 6.

Comparison of Fig. 6a with Fig. 6b also shows that, at any value of α for a given input power level, the higher propellant flow rate (0.6 g/s) case always requires a higher total spacecraft mass to transport the same payload than the corresponding case with a lower propellant flow rate (0.2 g/s).

Figure 7 shows the variation in the total time with input power at two different propellant mass flow rates for different values of α. It shows that the trip time decreases monotonically with increasing input power. Comparison of Figs. 7a and 7b also shows that there is an effective horizontal asymptote, and that the asymptote is lower for higher values of propellant flow rate. This is because of the higher value of thrust, at a given input power, due to a higher mass flow rate.

C. Constant Input Power

It is typically assumed that at a given power level, increasing the exhaust velocity will monotonically increase the trip time. Because

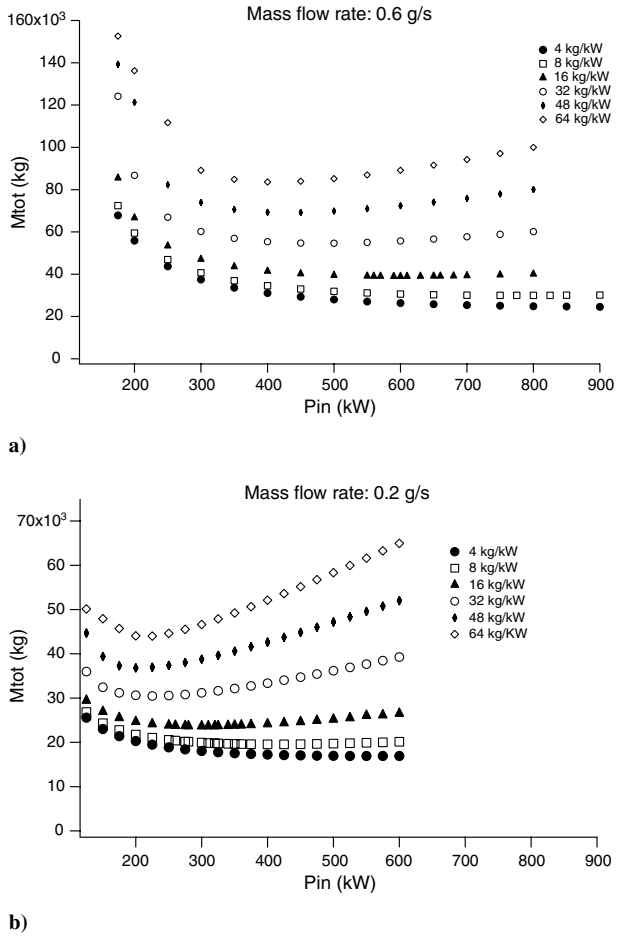

Fig. 6 Spacecraft mass vs the input power for two values of the propellant mass flow rate at different values of specific mass of the power plant.

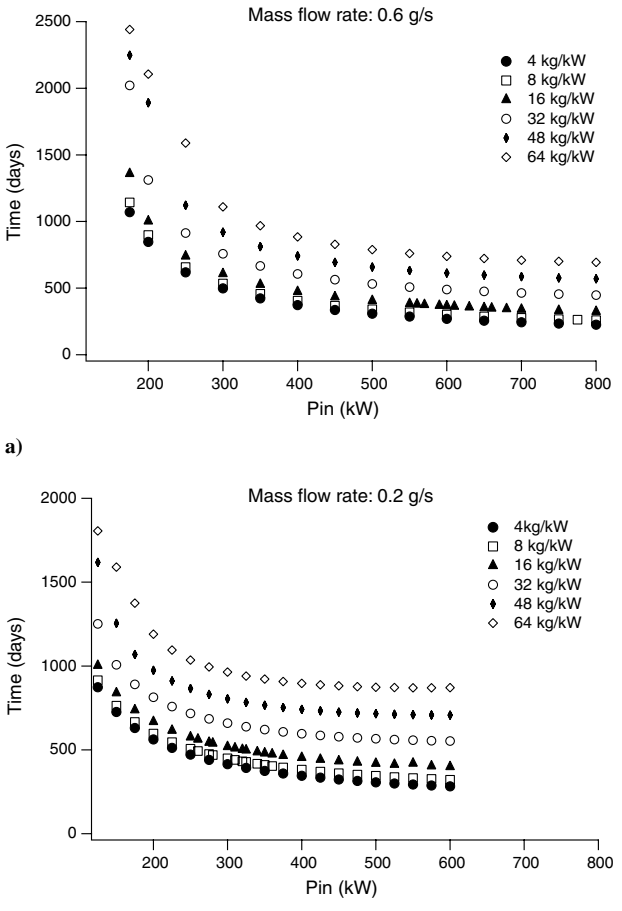

Fig. 7 Variation in trip time with input power at two values of mass flow rate for various values of specific mass.

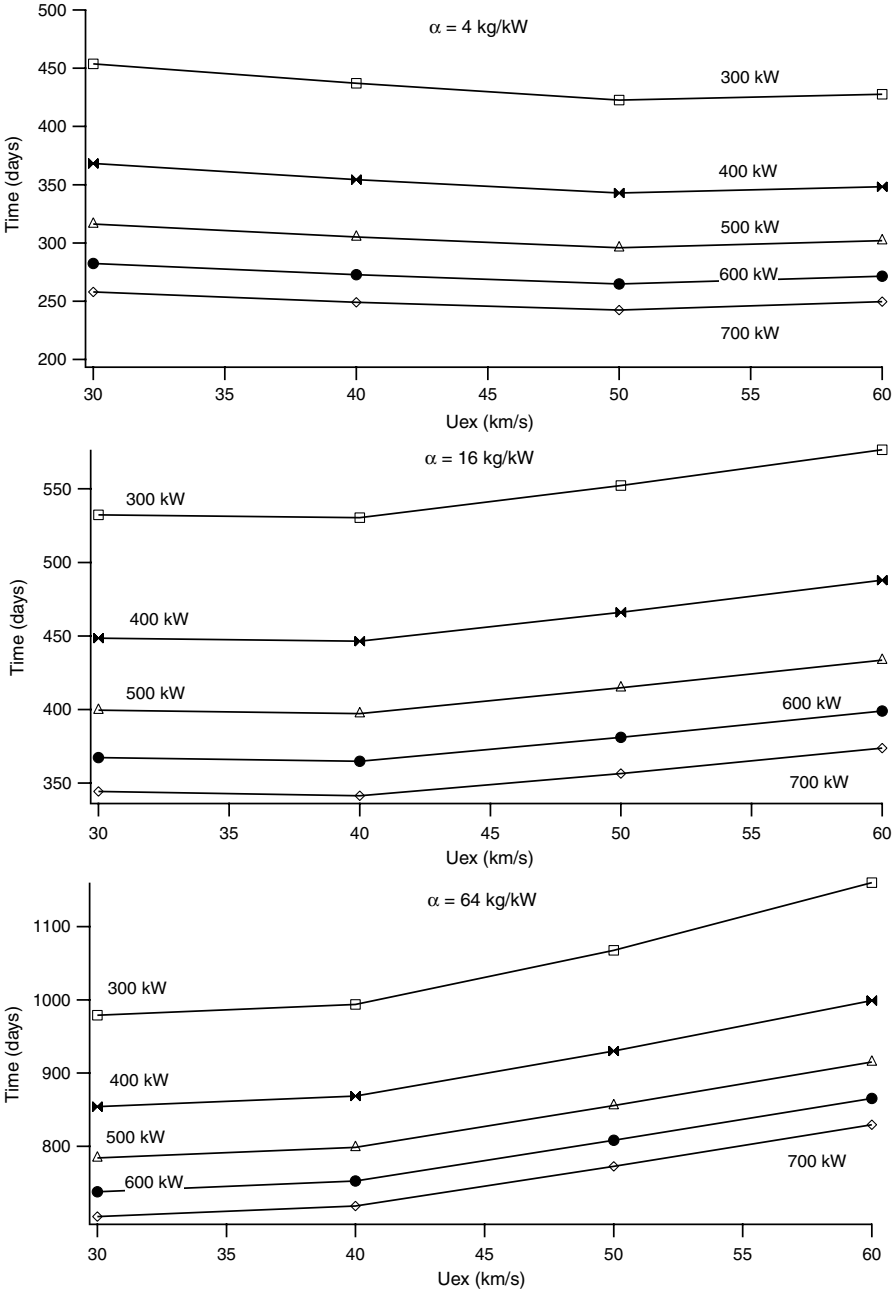

Fig. 8 Variation in trip time with exhaust velocity at different power levels for three values of specific mass.

$P_{\text{th}} = \frac{1}{2}Tu_{\text{ex}}$, increasing u_{ex} decreases T and is therefore expected to reduce the acceleration of the spacecraft and, consequently, increase the trip time. Figure 8 shows the variation in total time with exhaust velocity at different power levels for three different values of α. It shows that, contrary to expectation, the variation in trip time with exhaust velocity is not monotonic. The reason for this trend is that, up to a certain value of u_{ex} (which depends upon the value of α), the reduction in the fuel mass associated with increasing the exhaust velocity is more significant than the reduction in thrust, and this leads to a higher acceleration of the spacecraft. Beyond this value of u_{ex}, however, the reduction in fuel mass is not sufficient to compensate for the reduction in thrust and the acceleration of the spacecraft decreases.

Figure 8 also shows that the value of u_{ex} at which this trade-off occurs decreases with increasing value of α, because the power supply penalty becomes more significant at higher values of α. Note that Fig. 8 only indicates the existence of an optimum exhaust velocity that minimizes trip time but does not give the value of that optimum, because the discrete variation in exhaust velocity (limited by the data in Fig. 1), in steps of 10 km/s, is too large to give an optimum value accurately.

V. Conclusions

This study was intended to analyze the effect of variations in the performance of a LiLFA propulsion system on a cargo mission to Mars. To that end, we calculated the total spacecraft mass and the total trip time required to transport a fixed payload from Earth orbit to Mars orbit for 611 distinct combinations of α, P_{in}, η, and either u_{ex} or $\dot{m}$. It was not the goal of this study to accurately predict the optimum values of total spacecraft mass, trip time, or exhaust velocity, but only to study the trends in those quantities due to variation in propulsion system performance. We considered realistic ranges of values for relevant parameters that were reasonably close to experimentally demonstrated values, and we accounted for how some parameters, such as efficiency, depend on other parameters.

The results clearly show that the trip time monotonically decreases with increasing power. However, they also indicate a point of

diminishing return above which very large increases in input power are necessary for even modest decreases in trip time. Furthermore, it was also shown that, at a given power level and specific mass, the trip time was higher for higher exhaust velocities, and also that these variations increase with increasing specific mass. The results of variations in the total spacecraft mass with input power show the existence of an optimum input power at which the total mass required is at a minimum, for a given value of mass flow rate and specific mass. The results of the variation of the total spacecraft mass with the thruster exhaust velocity indicate an optimum exhaust velocity at each value of propellant flow rate and specific mass. At a given power level, the results indicate that the existence of an optimum exhaust velocity minimizes trip time as well. The total trip time decreases strongly with increasing efficiency and, unlike increases in u_{ex}, there is no optimum value beyond which the improvement is counterproductive. This indicates the importance of research into increasing the efficiency of the thruster.

Because of the inherently discrete nature of the variations in performance parameters in this study, the optimums (of exhaust velocity and the corresponding spacecraft mass) obtained were only approximate values. A future study could automate the variations to have finer resolution near the optimum values and refine those estimates. The specific mass of the power supply was assumed to be constant throughout the mission. For solar electric propulsion systems, the power obtained from the fixed mass of the power supply diminishes with increasing distance from the sun, and therefore it would be useful to perform a future study in which $\alpha(r)$. While this study revealed how mission parameters (trip time and total mass) varied with variations in performance parameters, the precise values of those mission parameters are not reliable because the planetary orbits were assumed to concentric circles. Furthermore, the estimates for the thrust angles [Eqs. (17–19)] are too simplistic, and though our calculation for Mars capture sets zero radial velocity at Mars orbit, a more sophisticated way to calculate these angles (such as the one used in [4]) is necessary to ensure that the relative velocity of the spacecraft is zero at Mars arrival. A future study that performs these calculations with more realistic planetary orbits and thrust angles would yield more reliable values for optimum exhaust velocity and optimum input power.

References

[1] Tsien, H. S., "Take-Off from Satellite Orbit," *Jet Propulsion*, Vol. 23, No. 4, 1953, p. 233.

[2] Stuhlinger, E., "Flight Path of an Ion-Propelled Space Ship," *Jet Propulsion*, Vol. 27, No. 4, 1957, p. 410.

[3] Jahn, R. G., *Physics of Electric Propulsion*, McGraw–Hill, New York, 1968.

[4] Chiravalle, V. P., "Nuclear Electric Ion Propulsion for Three Deep Space Missions," *Acta Astronautica*, Vol. 62, Nos. 6–7, 2007, p. 374.

[5] Sankaran, K., Cassady, L., Kodys, A. D., and Choueiri, E. Y., "A Survey of Propulsion Options for Cargo and Piloted Missions to Mars," *Annals of the New York Academy of Sciences*, Vol. 1017, 2004, pp. 450–467. doi:10.1196/annals.1311.027

[6] Oh, D. Y., "Development of a Simple Analytic Model for Optimum Specific Impulse Interplanetary Low Thrust Trajectories," *16th AAS/AIAA Space Flight Mechanics Conference*, AIAA, Reston, VA, 2006.

[7] Pennar, K. Z., Mikellides, P. G., and Ziemer, J. K., "Development of a Rapid Electric Propulsion System for Preliminary Design and Optimization Tool," *45th Joint Propulsion Conference*, AIAA, Reston, VA, 2009.

[8] Turchi, P. J., *Propulsion Techniques: Action and Reaction*, AIAA, Reston, VA, 1998.

[9] Fearn, D. G., "The Manned Exploration of Mars Using Nuclear Propulsion," *4th International Spacecraft Propulsion Conference*, ESA, The Netherlands, 2004.

[10] Polk, J. E., "Lithium-Fuelled Electromagnetic Thrusters for Robotic and Human Exploration Missions," *Space Nuclear Conference*, American Nuclear Society, La Grange Park, IL, 2005.

J. Martin
Associate Editor